

Rayment E. Moxley

Mark D. Adley

Bob Rohani

Structures Laboratory

US Army Waterways

Experiment Station

3909 Halls Ferry Road

Vicksburg, MS 39180

---

# Impact of Thin-Walled Projectiles with Concrete Targets

*An experimental program to determine the response of thin-walled steel projectiles to the impact with concrete targets was recently conducted. The projectiles were fired against 41-MPa concrete targets at an impact velocity of 290 m/s. This article contains an outline of the experimental program, an examination of the results of a typical test, and predictions of projectile deformation by classical shell theory and computational simulation. Classical shell analysis of the projectile indicated that the predicted impact loads would result in circumferential buckling. A computational simulation of a test was conducted with an impact/penetration model created by linking a rigid-body penetration trajectory code with a general-purpose finite element code. Scientific visualization of the resulting data revealed that circumferential buckling was induced by the impact conditions considered. © 1995 John Wiley & Sons, Inc.*

---

## BACKGROUND

Investigations into the survivability of hardened structures due to impact by conventional air-delivered munitions such as air-delivered bombs, have focused on defeating the bomb by casing failure. A traditional method of hardening structures against attack by aerial bombs is to place a burster slab over the structure. The burster slab is designed to detonate or break up contact-fused bombs and withstand penetration and blast effect of tail-fused bombs (Department of the Army, 1986). A concrete burster slab design was recently evaluated to investigate the effect of construction joints on the penetration resistance of the slab. Subscale thin-walled projectiles (simulating general purpose bombs) were fired into sections of the burster slab within a velocity range of 276–298 m/s. The penetration experiments were conducted at the US Army Engineer Waterways Experiment Station (WES) Projectile Penetration

Research Facility which accommodates large targets constructed under laboratory-controlled conditions (Frew et al., 1993). All projectiles broke up after partial penetration into the slab. This article presents a discussion of the test results, an analysis of the structural response of the projectile using classical shell theory, and an ABAQUS finite element simulation of the test (ABAQUS is available under license from Hibbitt, Karlsson, and Sorensen, Inc., 1989a, 1989b, 1989c).

## EXPERIMENTAL PROGRAM

Each target consisted of a conventional-strength concrete burster slab placed on a pumice shock-attenuation layer placed on a concrete slab simulating the roof of a structure. The 325-mm thick concrete burster slab, 350-mm thick pumice layer, and 152-mm thick concrete slab were

---

Received December 16, 1994; Accepted February 20, 1995.

Shock and Vibration, Vol. 2, No. 5, pp. 355–364 (1995)

© 1995 by John Wiley & Sons, Inc.

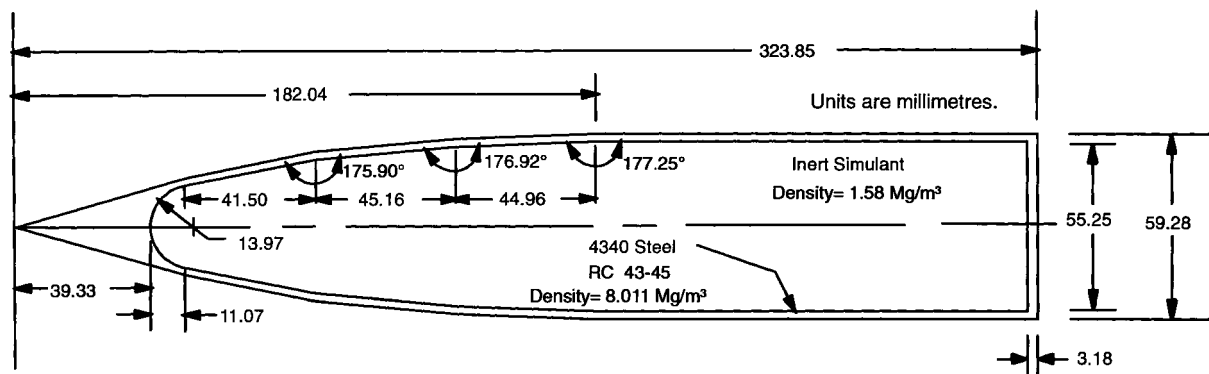
CCC 1070-9622/95/050355-10

placed in 2.14-m diameter culverts. The targets were cured for approximately 105 days prior to testing. Day-of-test breaks conducted on  $152 \times 305$  mm cylindrical specimens prepared when the targets were poured and tested per specifications (ASTM, 1994), indicated the concrete unconfined compressive strength was 41 MPa at test date. The projectiles used in the nine penetration tests were generic subscale models of a general purpose (GP) bomb. The projectiles were machined from 4340 steel, heat treated to a Rockwell C hardness of 43–45, and then remachined to their final dimensions. They were then filled with a grout material at a density of approximately  $1.57 \text{ Mg/m}^3$  to simulate the explosive filler and sealed by tapping in the end cap. A drawing of the subscale penetrator and its pertinent characteristics is shown in Fig. 1. The 59-mm diameter projectiles were fitted with three-piece polypropylene plastic sabots to carry them down the 83-mm caliber launch tube and fired horizontally into the targets. Figure 2 presents the projectile with its sabot.

## TEST RESULTS

The projectile impacted the burster slab between 276 and 298 m/s. The average velocity was 288

m/s. Impact conditions were consistent with normal impact [see Fig. 3(b,c)]. The total penetration depth into the burster slab ranged from 73 to 143 mm. The average penetration depth was 117 mm. A typical drawing of the target depicting target damage is presented in Fig. 3. All of the projectiles broke in a similar manner. Typically, the broken pieces of the projectile included the nose and seven to nine long strips from along the aftbody of the projectile. Figure 4 presents posttest photographs of a broken projectile viewed from the nose and through a cross section. Examination of the pieces of a broken projectile indicate that the projectile shell underwent severe deformation at about 89 mm from the nose tip or about the distance the nose was embedded in the burster slab. Examination of the projectile noses revealed plastic deformations consistent with the application of a large external pressure. The projectile noses displayed seven to nine longitudinal cracks in the region where the nose was sheared from the aftbody. Fracturing of the projectile was presumably initiated by these longitudinal cracks which then propagated toward the aftbody resulting in splitting of the aftbody into seven to nine strips. The edges of the metal strips were aligned with the longitudinal cracks observed on the intact portion of the nose. The seven to nine metal strips formed by fracturing of the aftbody were bent into a circular shape [Fig. 4(b)].



### Pertinent Characteristics for Subscale GP Bomb

- Total Mass: 1.962 kg
- Simulant-to-Mass Ratio: 0.506
- CG Location: 190 mm from nose tip
- Transverse Moment of Inertia:  $0.01446 \text{ kg}\cdot\text{m}^2$

FIGURE 1 Drawing of the projectile used in the penetration tests and its pertinent characteristics.

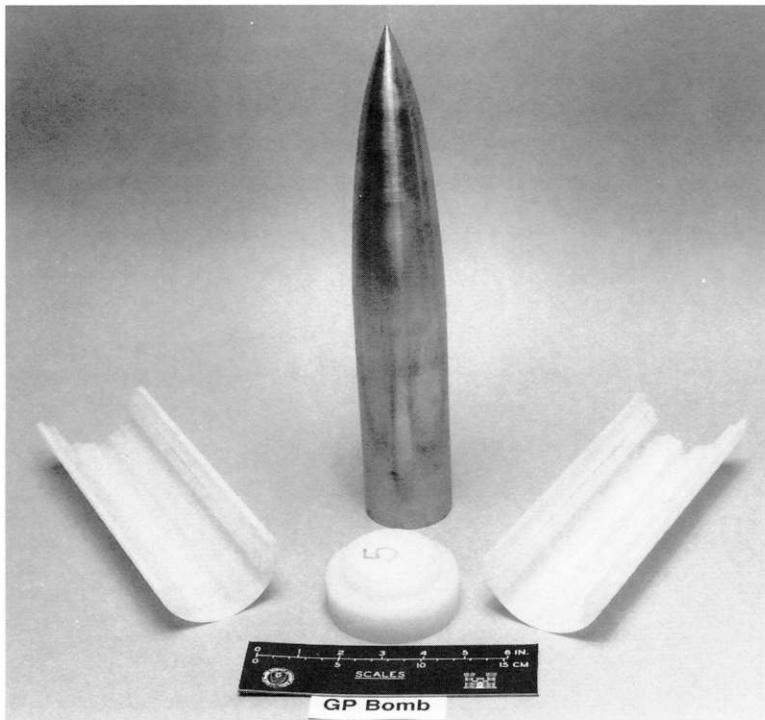


FIGURE 2 Finished projectile with three-piece sabot.

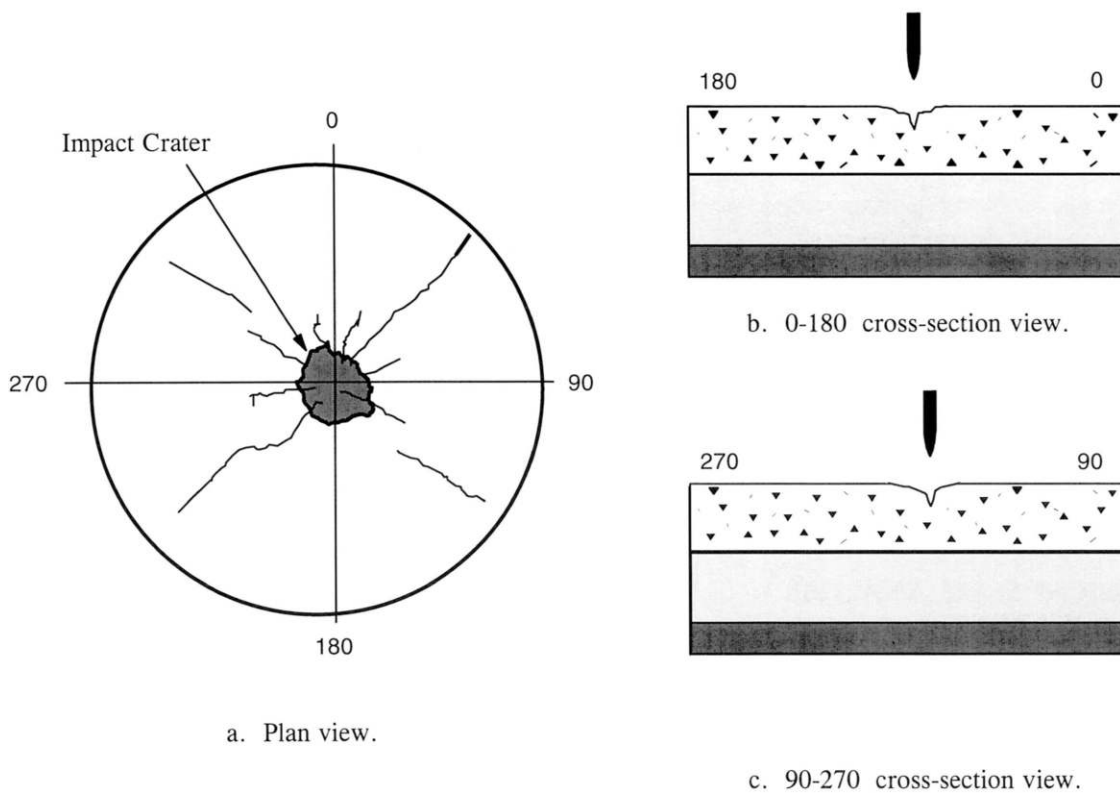
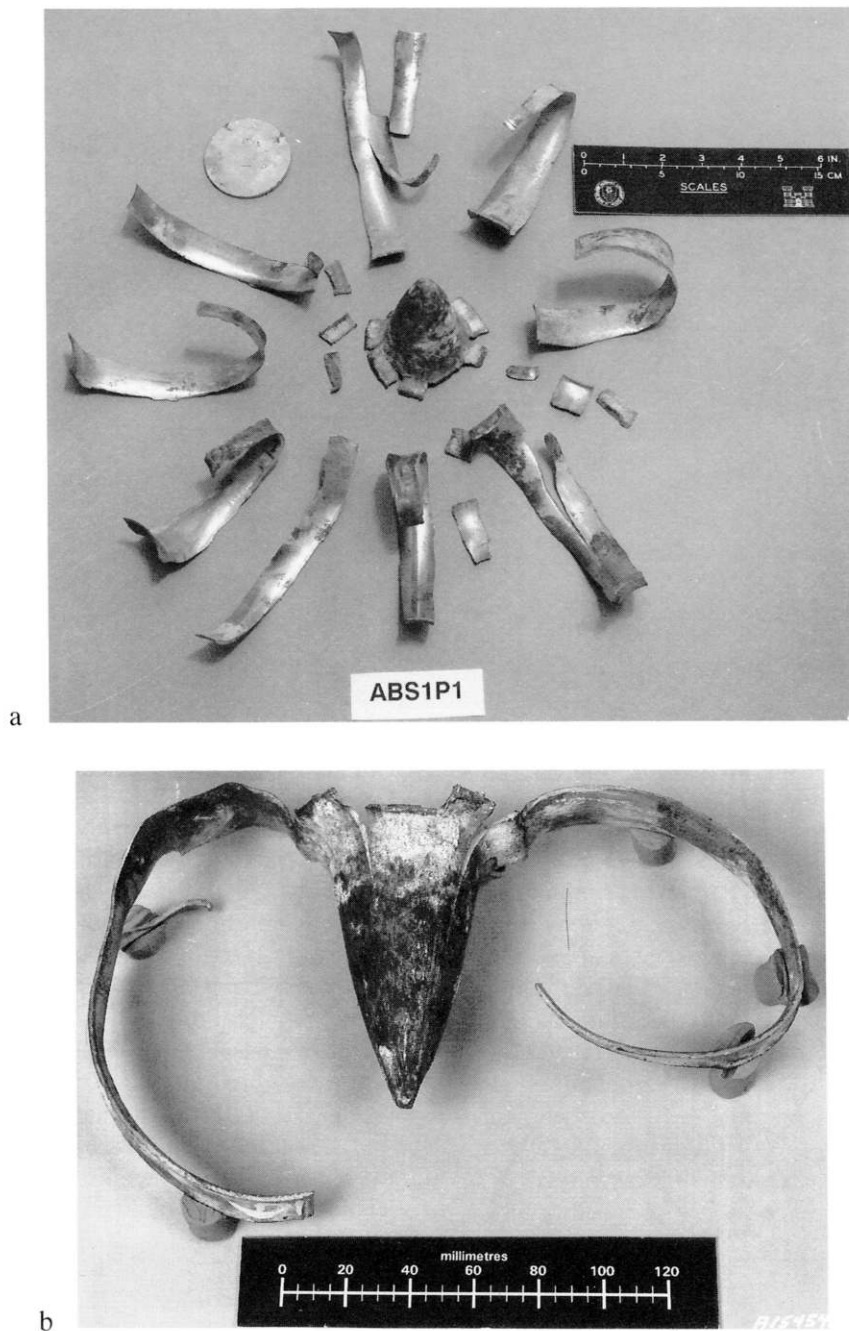


FIGURE 3 Plan and section views of posttest target damage: (a) plan view; (b) 0–180° cross-section view; (c) 90–270° cross-section view.



**FIGURE 4** Views of posttest damage to projectile: (a) view from nose and (b) typical side view.

### CLASSICAL SHELL ANALYSIS OF PROJECTILE

Structural failure of thin-walled projectiles during impact and subsequent penetration into a hard target (such as concrete) is of great interest to weapon designers as well as to the protective construction community. In practice most of the failures take place under oblique impact due to

projectile rotation that results in tail-slap with the target. Under normal impact, however, failure is due to shell buckling and symmetrical splitting of the aftbody of the projectile.

Buckling of thin shells has been studied extensively in Timoshenko and Gere (1961) and two modes of buckling has been identified. Axial (or longitudinal) buckling that takes place under critical axial stress given by

$$\sigma_{cr} = \frac{Eh}{a\sqrt{3(1-\nu^2)}} \quad (1)$$

where  $E$  and  $\nu$  are the Young's modulus and Poisson's ratio of the steel shell, and  $h$  and  $a$  are the thickness and radius of the shell, respectively. It is pointed out in Timoshenko and Gere (1961) that buckling actually takes place at much lower stress than predicted by the theoretical value given by Eq. (1). On the basis of experimental data, the following empirical equation is recommended in Timoshenko and Gere for calculating the buckling load

$$\sigma_{ult} = E \frac{0.6 \frac{h}{a} - 10^{-7} \frac{a}{h}}{1 + 0.004 \frac{E}{\sigma_{yp}}} \quad (2)$$

where  $\sigma_{yp}$  is the yield stress of the shell material. The second mode is circumferential buckling which is caused by the critical lateral (radial) stress

$$q_{cr} = \frac{Eh^3(n^2 - 1)}{12a^3(1 - \nu^2)} \quad (3)$$

where  $n$  specifies the buckling mode ( $n$  is the number of waves); i.e.,  $2n$  is the number of sine curve half-waves formed by the circumference of the shell in buckling. Experimental data show lower values for  $q_{cr}$  than predicted by Eq. (3),

and it is recommended that the minimum critical pressure should be  $0.8q_{cr}$  (Young, 1989). To use Eqs. (2) and (3) to forecast the onset of buckling, the axial and radial stresses experienced by the projectile during the penetration process must be calculated. For the penetration depth achieved during the experiment [Fig. 5(a)], the average resisting force can be obtained from integration of the equations of motion and is given as

$$F_{ave} = \frac{WV_o^2}{2gP} \quad (4)$$

where  $W$  is the weight of the projectile,  $V_o$  is the impact velocity,  $P$  is the maximum depth of penetration, and  $g$  is the acceleration due to gravity. The axial stress experienced by the shell due to this force is simply [Fig. 5(b)]

$$\sigma_{axial} = \frac{WV_o^2}{2gP} \frac{1}{2\pi ah} \quad (5)$$

The radial stress on the nose of the projectile that will result in  $F_{ave}$  is [Fig. 5(c)]

$$\sigma_{radial} = \frac{WV_o^2}{2gP} \frac{1}{\pi a^2} \quad (6)$$

Axial buckling will take place if  $\sigma_{axial} \geq \sigma_{ult}$ . Circumferential buckling will take place if  $\sigma_{radial} \geq 0.8q_{cr}$ . The numerical values of the parameters of the shell and penetration data can be substi-

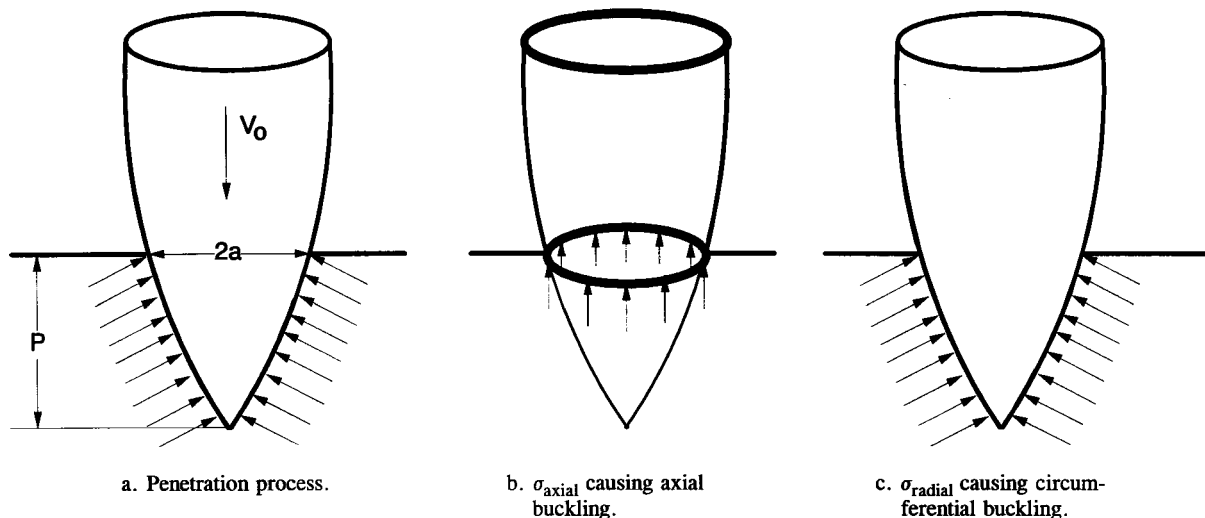


**FIGURE 5** Penetration process, axial, and radial stresses inducing buckling: (a) penetration process; (b)  $\sigma_{axial}$  causing axial buckling; (c)  $\sigma_{radial}$  causing circumferential buckling.

tuted in Eqs. (2)–(6) to forecast the possibility of buckling. Following through the analyses results in:  $\sigma_{\text{axial}} = 1786$  MPa;  $\sigma_{\text{ult}} = 6848$  MPa;  $\sigma_{\text{radial}} = 327$  MPa;  $0.8q_{\text{cr}} = 11.2 (n^2 - 1)$  MPa. This indicates that axial buckling will not take place, but the shell will undergo circumferential buckling with four to six waves just due to the average radial stress. The maximum radial stress experienced by the projectile is higher than the average value and can be calculated from analytical penetration models (Luk and Forrestal, 1987; Forrestal and Longscope, 1990). Assuming an elastic–plastic constitutive model for concrete, the maximum radial stress for  $V_o = 290$  m/s varies from 15 to 20 times  $f'_c$  depending on concrete properties ( $f'_c =$  unconfined compressive strength = 41.4 MPa for the target concrete used in the penetration test). This indicates that the maximum value of radial stress may vary from 621 to 828 MPa, which would cause circumferential buckling with eight waves. It should be pointed out that the maximum value of radial stress is still below the stress necessary to induce axial buckling.

## COMPUTATIONAL SIMULATION

The PENCURV/ABAQUS (Adley, 1993) impact/penetration code used in this article was created by utilizing required sections of the PENCURV (Berger and Adley, 1994) rigid-body trajectory code as the heart of an ABAQUS (Hibbitt, Karlsson, Sorensen, Inc., 1989a, 1989b, 1989c) DLOAD user subroutine. (PENCURV/ABAQUS denotes the code created by using the logic and forcing functions of the trajectory code PENCURV as an ABAQUS DLOAD user subroutine; it is not a product of, and it is not endorsed by Hibbitt, Karlsson, and Sorensen, Inc.) Because ABAQUS integrates the equations of motion to determine the projectile's current deformed shape, position, velocity, and acceleration, the PENCURV section of the ABAQUS DLOAD user subroutine is only required to perform the following computational tasks: read input data that describes the configuration of the target (only on the first call to the DLOAD user subroutine); determine whether or not each element Gauss point is in contact with the target; check for free-surface and interface effects; and compute the magnitude of the normal stress at each element Gauss point that is in contact with the target.

The impact/penetration code PENCURV/ABAQUS represents an alternative approach to penetration problems. This approach does not require modeling of the target or a separate analysis to determine the penetration loads and in many cases it is less time-consuming and less expensive than fully coupled or uncoupled methods of analyses. Also, because the deformation of the projectile at a given time step is allowed to influence the loads obtained from the trajectory code at the next time step, this approach represents a simply coupled method of analysis.

The nodal coordinates of the projectile finite element model define the initial position and orientation of the projectile. The element type and connectivity define the structural shape of the projectile, and the position and orientation of the projectile's surface. The correct mass, center of gravity, and mass moment of inertia of the projectile are obtained by utilizing several materials that are identical except for the value of their densities, i.e., the mass of internal components is accounted for by utilizing these artificial density values. Thus, the interactions of the filler material with the shell of the projectile are not explicitly accounted for in this formulation. The initial (impact) velocity vector of the projectile is defined by specifying the initial velocity of the translational degrees of freedom at each nodal point of the finite element model. Material nonlinearities are accounted for by specifying that a Mises yield surface with associated plastic flow and isotropic hardening be used for the projectile elements. To account for geometric nonlinearities the NLGEOM option is specified in the ABAQUS solution procedure description.

## PENCURV/ABAQUS IMPACT/PENETRATION ANALYSES—NORMAL IMPACT INTO CONVENTIONAL-STRENGTH CONCRETE

The problem under consideration investigates the structural response of a thin-walled projectile as it impacts and penetrates the concrete and pumice layered target previously described. The impact conditions specified were consistent with normal impact [see Fig. 3(b,c)]. The impact speed, or magnitude of the velocity vector, of the projectile is assumed to be 290 m/s. The projectile is composed of material that is assumed to obey an elastic–plastic material law with an initial yield stress of 1324 MPa. The concrete layers are assumed

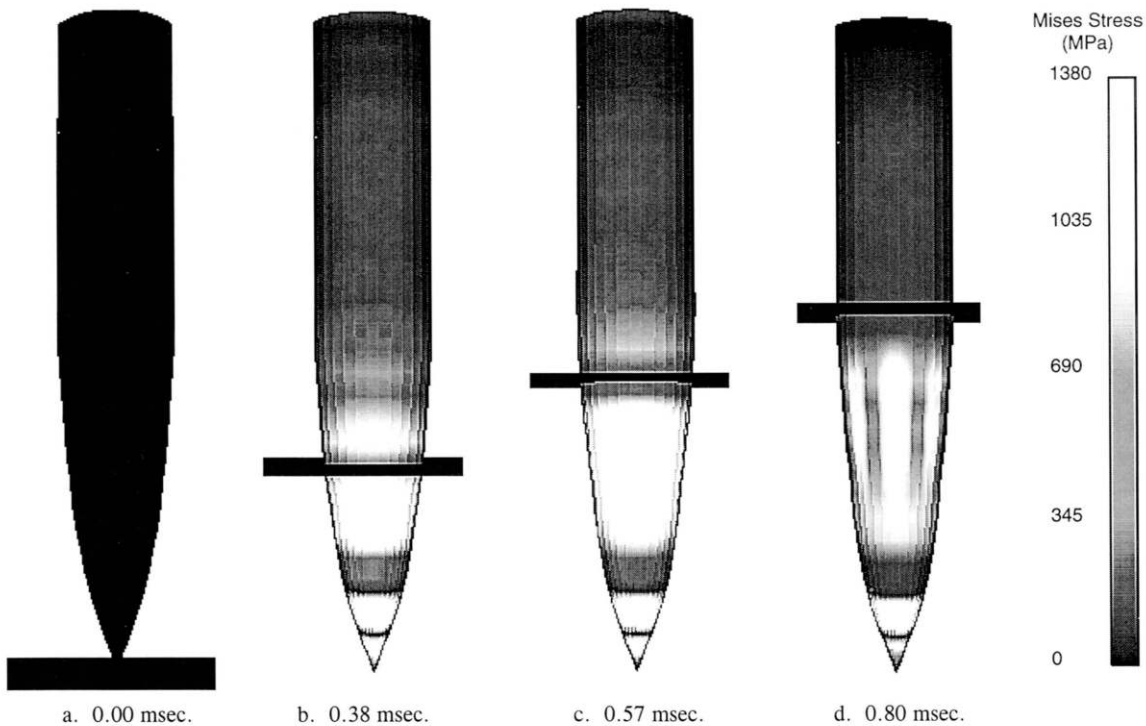


**FIGURE 6** Mises stress shown on deformed shape: (a) 0.00 ms; (b) 0.38 ms; (c) 0.57 ms; (d) 0.80 ms.

to have an unconfined compressive strength of 41.4 MPa and a mass density of 2.4 Mg/m<sup>3</sup>. The pumice layer is assumed to have a mass density of 0.497 Mg/m<sup>3</sup>.

Figure 6 contains plots of the deformed shape of the projectile at 0.00, 0.38, 0.57, and 0.80 ms after impact; a scale factor of 1.0 was used for this plot. The large flat element shown in Fig. 6 represents the surface of the target. The vertical distance between the large element and the nose of the projectile represents the penetration depth at the time step considered in the plot.

An examination of Fig. 6 reveals that significant levels of Mises stress are imposed on the projectile by the impact/penetration loads, e.g., at 0.57 ms after impact a large region of the projectile's nose is subjected to Mises stresses of approximately 1380 MPa. This leads to the conclusion that if the projectile under consideration were subjected to those impact conditions, it would sustain significant permanent damage, i.e., significant levels of plastic strain. The finite magnitude of the structural deformations shown in Fig. 6(c,d) also support that conclusion. Further examination of Fig. 6 also reveals that the distribution of the Mises stress is axisymmetric for the first 0.57 ms of the impact event. This axisymmetric stress distribution is consistent with the loads

resulting from a normal impact event. The nonaxisymmetric distribution of Mises stress shown in Fig. 6(d) is indicative of a displacement field that would result from circumferential buckling.

Figure 7 shows a comparison between the projectile's undeformed shape and its deformed shape at 0.60 ms; a scale factor of 2.0 was used for this plot. The deformations shown in Fig. 7 are consistent with the fact that the nose of the thin-walled projectile is hollow, and with the fact that the normal impact loading event is tantamount to the application of a large external pressure load to the projectile's nose. This mode of deformation is also observed in the impact experiments, i.e., the intact portion of the projectile's nose sustained permanent plastic deformations consistent with the deformation mode shown in Fig. 7.

Figure 8 shows the deformation of a cross section of the projectile that is located just aft of the projectile's nose; a scale factor of 20.0 was used for this plot. An examination of Fig. 8 reveals that the displacement field is consistent with circumferential buckling where the buckling mode consists of eight full waves (or 16 half-waves). It should be noted that the buckling mode predicted in the numerical simulation is in agreement with the analytical analysis presented in the previous



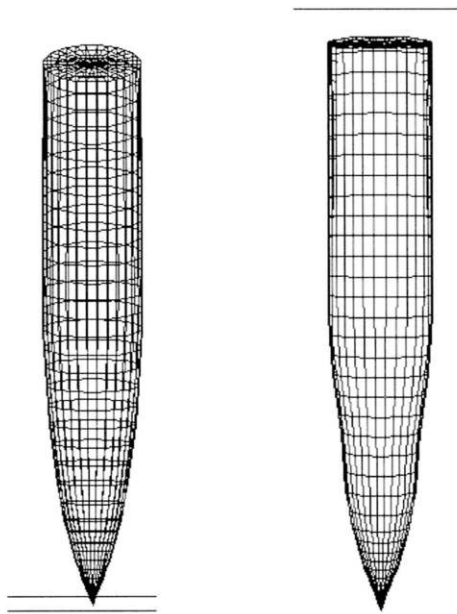


**FIGURE 7** Undeformed and deformed shape at 0.60 ms after impact (scale factor = 2.0).

section, i.e., the analytical analysis also predicted that the peak loads imposed by the impact event were sufficient to cause circumferential buckling with a buckling mode that consists of eight full waves in the circumferential direction. An examination of the stresses on the inner surface of the shell reveals that this mode of deformation results in the creation of eight zones of high Mises stress separated by eight zones of lower Mises stress; these are caused by the reversals of curvature in the circumferential direction. It should be noted that if the stresses on the outer surface of the shell are examined, the locations of the high and low Mises stresses in Fig. 8 would be reversed. This fact might initially lead one to conclude that there are 16 points of stress concentration along the circumference that would lead to a failure mode consisting of 16 fractures. However, it is important to consider the interaction of the filler with the projectile shell when attempting to forecast the actual postbuckling failure mode of the projectile. The filler material resists shell displacements that are directed inward while magnifying displacements that are directed outward. Therefore, the curvature and the stresses will be higher along the peak of the eight half-waves that are directed outward. This consideration of the interaction of the filler and the shell indicates that the predicted buckling mode will lead to a postbuckling failure configuration that consists of the

formation of eight fractures. It is important to note that the failure mode of the test projectiles is consistent with this conclusion, i.e., the body of the projectile fractured into eight strips. The eight strips could have been formed by cracks that developed at the eight stress concentrations created by the interaction of the filler material with the buckled shape of the shell.

Figure 9 shows the distribution of  $Y$ -normal stress, stress in the direction of the longitudinal axis of the projectile, at 0.37 ms after impact. For sections of the projectile where its surface is parallel to that axis, i.e., the aftbody, the  $Y$ -normal stress corresponds to the axial stress. The values of  $Y$ -normal stress shown in Fig. 9 were the largest observed during the impact/penetration event. It should be noted that the maximum value of 966 MPa shown in Fig. 9 is less than the critical longitudinal buckling load computed in the previous section. Thus, the fact that longitudinal buckling is not present in the numerical simulation is consistent with the classical analysis of the previous section.

The axial stress levels computed in the classical analysis are larger than the values predicted in the numerical simulation. This is explained by noting that the maximum depth of penetration predicted in the simulation is 175 mm versus the value of 117 mm used for the classical analysis (the penetration depths observed in the tests ranged from 73.4 to 143.2 mm). The higher value of penetration depth predicted by the numerical



**FIGURE 8** Cross-sectional view of projectile 0.80 ms after impact revealing circumferential buckling mode (scale factor = 20.0).



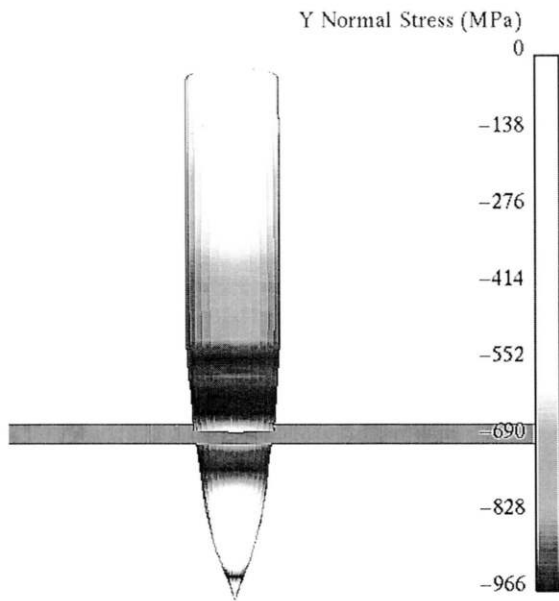


FIGURE 9 Distribution of Y-normal stress (MPa).

simulation is partially a result of the fact that the numerical model is not able to simulate projectile fracturing, i.e., a deformed but intact projectile would be expected to penetrate deeper than eight separate strips of steel. Evidence of circumferential buckling in the simulation is first noted at 0.68 ms after impact, at which time the penetration depth is 160 mm. Because the onset of circumferential buckling is suspected to coincide with the onset of fracture, penetration predicted by the simulation subsequent to circumferential buckling (15.2 mm in this example) is probably not realistic, but rather just a result of not modeling projectile fracturing. It should also be noted that the simulation was able to capture the circumferential buckling without any interference from the analyst, i.e., without the analyst perturbing the shell geometry, the displacement field, or the distribution of the applied loads. If the aforementioned perturbations had been utilized to model the effect of shell imperfections, heterogeneous target material, etc., circumferential buckling may have been detected earlier in the solution; this would tend to make the penetration depth at the onset of buckling agree even more closely with the penetration depths observed in the experiments.

## SUMMARY AND CONCLUSIONS

The results of the experiment, classical shell analysis, and finite element analysis all indicate that

the projectile failed in a circumferential buckling mode. The classical analysis and the numerical simulation indicate that the axial load experienced by the projectile was significantly less than the ultimate axial stress required to cause axial buckling in a cylinder. Radial compression of the projectile nose and circumferential buckling of the shell approximately 89 mm from the nose tip, predicted with PENCURV/ABAQUS simulation, were consistent with the experimentally observed results. The development of longitudinal cracks in the region of circumferential buckling, and fracturing of the aftbody into seven to nine strips experimentally observed, although not explicitly predicted in the PENCURV/ABAQUS simulation, were forecasted based on the calculated stress levels. The total penetration depth predicted with PENCURV/ABAQUS was greater than the maximum depth observed in the experiments. Taking into consideration the time at which the projectile began to experience circumferential buckling, the penetration depth forecast by PENCURV/ABAQUS was close to the maximum value observed in the actual tests. The recently developed PENCURV/ABAQUS impact/penetration code utilized herein appears to be an effective method for determining the structural response of projectiles subjected to impact/penetration loading events. Future efforts will include a numerical simulation that explicitly accounts for the interaction of the filler material with the projectile shell. Additional tests and analysis are planned to examine the shell failure mode due to impact with high-strength rock material that will take advantage of improved diagnostics such as flash x-ray and high-speed digital imagery. This future work will allow us to determine with greater certainty the dominant failure mechanisms present in the impact of thin-walled projectiles with concrete and rock targets.

The research reported herein was conducted as a part of the US Army Corps of Engineers (USACE) Hardened Design Technology Work Package, Work Unit No. AT40-HS-001 "Shielding Methodologies to Defeat Advanced Munitions." The permission from the Office, Chief of Engineers, to publish this article is gratefully acknowledged.

## REFERENCES

- Adeley, M. D., 1993, "A Simply Coupled Penetration Trajectory/Structural Dynamics Model," *Proceedings of the Sixth International Symposium on the*

- Interaction of Nonnuclear Munitions with Structures*, Panama City, FL, pp. 18–22.
- American Society for Testing and Materials, 1994, *1994 Annual Book of ASTM Standards*, Designation: C39-93a Standard Test Method for Compressive Strength of Cylindrical Concrete Specimens, ASTM, Philadelphia, PA.
- Berger, R. P., and Adley, M. D., 1994, “Two-Dimensional Projectile Penetration into Curvilinear Geologic/Structural Targets: PENCURV,” *Proceedings of the 65th Shock and Vibration Symposium*, San Diego, CA, to appear.
- Department of the Army Technical Manual, 1986, *TM5-855-1, Fundamentals of Protective Design for Conventional Weapons*, Headquarters, Department of the Army, Washington, DC (Available from National Technical Information Service, 5285 Port Royal Road, Springfield, VA).
- Frew, D. J., Cargile, D., and Ehrigott, J. Q., 1993, “WES Geodynamics and Projectile Research Facilities,” AMD-Vol. 171, *Proceedings of the Advances in Numerical Simulation Techniques for Penetration and Perforation of Solids*, ASME, pp 1–8.
- Forrestal, M. J., and Longcope, D. B., 1990, “Target Strength of Ceramic Materials for High-Velocity Penetration,” *Journal of Applied Physics*, Vol. 67, pp. 3669–5672.
- Hibbitt, Karlsson, and Sorensen, Inc., 1989a, *ABAQUS USERS MANUAL*, Version 4-8, Providence, RI.
- Hibbitt, Karlsson, and Sorensen, Inc., 1989b, *ABAQUS THEORY MANUAL*, Version 4-8, Providence, RI.
- Hibbitt, Karlsson, and Sorensen, Inc., 1989c, *ABAQUS EXAMPLES MANUAL*, Version 4-8, Providence, RI.
- Luk, V. K., and Forrestal, M. J., 1987, “Penetration into Semi-Infinite Reinforced-Concrete Targets with Spherical and Ogival Nose Projectiles,” *International Journal of Impact Engineering*, Vol. 6, pp. 291–307.
- Timoshenko, S. P., and Gere, J. M., 1961, *Theory of Elastic Stability*, McGraw-Hill, New York, pp. 457–519.
- Young, W. C., 1989, *Roark's Formulas for Stress & Strain*, McGraw-Hill, New York, pp. 690.



**Hindawi**

Submit your manuscripts at  
<http://www.hindawi.com>

